Refractive Index Sensor for Salty and Sugary Solution Based on Optical Fiber Technical

Refractive Index Sensor for Salty and Sugary Solution Based on Optical Fiber Technical

Maher Khaleel Ibrahim[1], Shehab A Kadhim[2] and Nabeil Ibrahim Fawaz[1]

[1]Department of Physics, College of Science, University Of Anbar.
[2]Laser & Optoelectronics Research Center, Ministry of Science & Technology.

E-mail: mkibrahim@uoanbar.edu.iq

Abstract. In this work, based on Mach- Zehender Interferometry (**MZI)** technique, a single-mode optical fiber had been designed as a water pollution sensor. The submitted sensor had been designed to detect pollutants in water. The sodium chloride salt and sugar were used as simulation examples of pollutants with different concentrations (0-0.45) mol /liter. The performance of the submitted sensor had been studied for different sensor arm diameters which were (63.5, 51.58, 39.68 and 20 μm). The variation of the refractive index of salty and sugary solutions surrounding the sensor leads to a change in the optical properties of the transmitted signal. In this work, a wavelength shifting had been obtained due to this variation. The influence of sensor diameter on the sensitivity of the system had been studied. From the results, we found that the higher sensitivity was for the sensors with a diameter of 20 μm, and they were 1130 pm/mol.l^{-1} and 1205 pm/mol.l^{-1} for salty and sugary solution respectively.

Keywords: optical fiber sensors, RI sensor, evanescent field, MZI, chemical etching, water pollution

1. Introduction

Related to the toxic effects the pollutants may have on humans, accurate measures of chemical species in water have increasingly gained functional significance. In this context, it is important to build up simple, responsive, low-cost, and portable water pollution sensors capable of direct measurements. Optical fiber technology provides many benefits for chemical sensing over traditional methods [1]. Compared to traditional devices, fiber optic sensor systems provide various advantages, including immunity to electromagnetic interference, lightweight and portable size, sensitivity, multiplex ability, remote sensing, and the most significant benefit is the ability to be built into the textile structure. An effective medium to sense chemical species is created by optical fibers. Light properties including intensity, phase, or polarization in the optical fiber may be modulated by the presence of chemical species. At the fiber output, these modulations can be observed and correlated with the concentration of the chemical species presented at the point. [2]

Any optical fiber consists of two dielectrics that are concentrically arranged: the center (core) and the cladding. A higher refractive index than the cladding is distinguished by the core [3]. Using HF as the etching agent is one of the simple methods used to make tapers. If the fiber is etched, as the fiber diameter is limited, the conditions controlling the transmission of light within the fiber change. It should also be remembered that the etching procedure is limited to a particular fiber length to achieve desired etched length and desired contact area [4]. In that configuration, it defines light propagation dependent on a total internal reflection. In the form of modes in the center and a small portion of energy penetrating the cladding known as the evanescent field, light is propagated. As a result, an exponentially greater cross-section of the cladding fills the area of the simple mode until it reaches the point where it is directed across its entire cross-section. A progressively greater cross-section of the cladding occupies the area of the simple mode until it reaches the point where it is directed in its cross-section. The change in boundary conditions is also closely associated with the change in the dimensions of the optical fiber. The light at the core/cladding interface is not propagated, but the air/cladding interface is propagated. The approximations used in the typical optical fiber mode solutions where the difference in refractive indices is small (less than 1%) are not valid. In this case, the light beam continues to be exposed and affected by the fiber surrounding air for tapered optical fibers where the light beam propagates in a whole system (as a core) and the environment becomes a cladding, as seen in Figure 1 [3]. As the optical fiber becomes more sensitive to external changes in the refractive index of the material surrounding the fiber, this method enables one to use additional material in an etched environment, especially in the tapered waist region. These links to different materials have been commonly used for the construction of sensors, filters, and amplifiers [5,6].

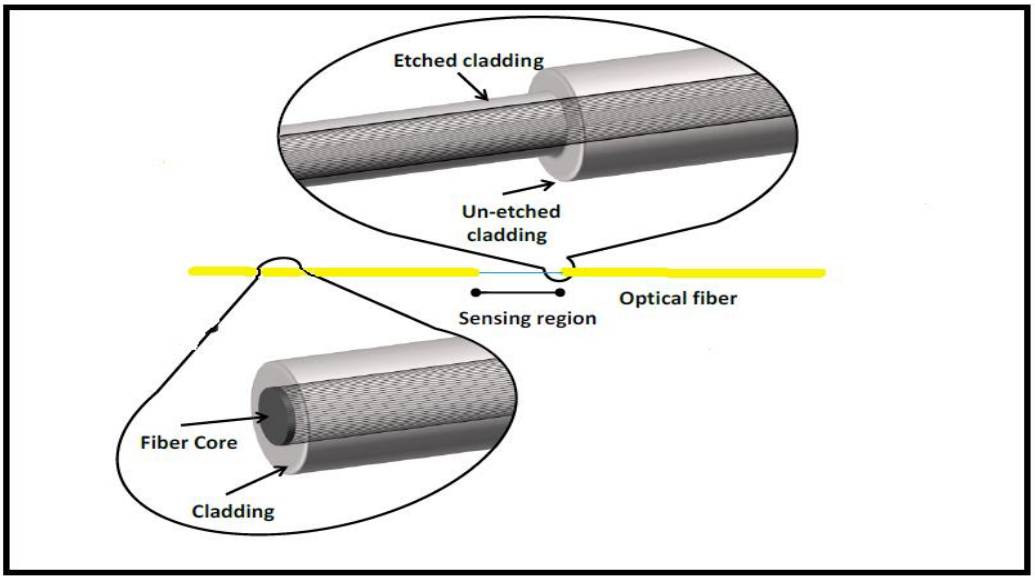

Figure 1. The schemes of the etched and non-etched region of optical fiber [7]

In biological fields, medicine and environment, optical fiber refractive index (RI) sensors are used. Many fiber optic RI sensors, such as Mach-Zehnder (MZIs), Fiber Grating, Fabry-Pérot (FPIs), Sagnac, and multi-mode interferometers have been published in the literature so far [8].
In particular, (MZIs) interferometers obtain from high sensitivity, a high degree of integration, accessibility and design compactness. Several optical fiber refractometers have recently been documented to allow the refractive index and many other parameters to be calculated simultaneously. These optical fiber instruments serve as evanescent wave sensors based on multimode interference systems, enhancing the dependency on high-order mode propagation constants on the external medium's refractive index to monitor changes in the environment's optical properties [9].

Many research groups submitted many research papers to solve many problems related to this very important topic.

James et al 2017 [10] stated that by depositing a nanoscale coating of titanium dioxide containing porphyrin as a functional material onto a tapered optical fiber, a highly sensitive ammonia sensor was developed. As a result of the interaction between porphyrin and ammonia, the difference in the refractive index of the coating material caused a change in the middle wavelength of the large-mode resonance, allowing the identification of ammonia concentrations in water as low as (0.1) ppm, with a reaction time of less than 30 sec. **Also, Devi et al 2018** [11] detected arsenic components in a drinking water, and MZI based on optical fiber was developed. The developed sensor is distinguished by its cost-effective, small, and laboratory-on-chip manufacturing capability. **In 2019 Ahsani et al** [12] a uniformly tapering SMF standard for MZI-based RI measurement was established. There are various applications in chemical and biochemical sensing fields for the suggested cheap and highly sensitive optical fiber RI sensors. **Finally in 2020 Ferria** [13] tested the distilled water solution mixed with methylene blue (MB), and an unclad optical fiber sensor was manufactured. At the core – liquid cladding interface, the manufactured sensor is based on evanescent wave absorption by the surrounding medium. Ferria concludes that the results showed that the designed sensor provides an effective response to the (6–50) mg / L concentration range.

In this work, an MZI sensor based on SMF had been designed for environmental applications. Sugary and salty liquids with different concentrations were employed as a simulation of water pollution. Moreover, the influence of the sensing arm diameter on sensor performance has been studied.

2. Experimental

The experiment was carried out using a section of the commercially available SMF of cladding and core diameter of (125 and 9) μm respectively.

About 3 cm length of the middle region of SMF was stripped and cleaned very well. After that, this section was immersed into Hydrofluoric acid (HF) to be chemically etched, that is to say, reducing its diameter to the desired value. The concentration of HF acid before dilution was 48%, and this strong acid has been diluted with distilled water to a ratio of (1 mm^3 HF: 1 mm^3 distilled water). The etching process took place at room temperature and the required cladding diameters have been achieved at etching times of (60, 90, 20 and 150) min. Then, the etched area had been cleaned very well using distilled water to remove any acid residuals.

Figure 2 below shows the MZI optical fiber sensor. A signal from the light source (single-mode fiber pigtailed Laser diode source -Thorlabs of center wavelength 1550 nm, and power 1.5 mW) was split by 2x1optical coupler (50/50) into two signals. The first signal goes to the reference arm while the second goes to the sensor arm. Then, both arms were collected using another 2x1 optical coupler. The output port was connected to Optical Spectrum Analyzer (THORLABS 203) with a wavelength range of 1000 to 2600 nm, and a resolution of 0.1 nm.

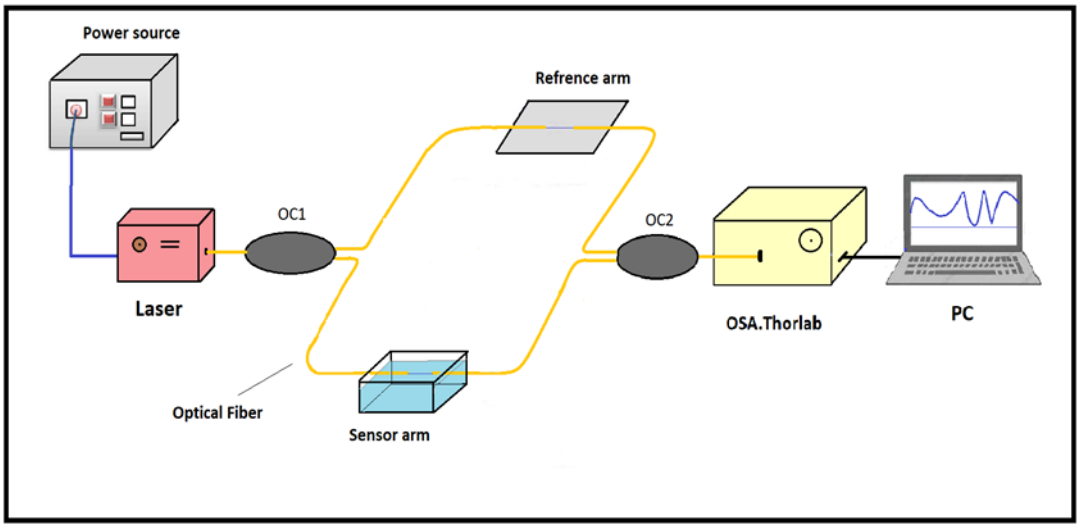

Figure 2. Schematic diagram of MZI- RI sensor

The tested solutions of sodium salt and sugar were prepared at different concentrations using the following equation:

$$C = \frac{m}{V} \times \frac{1}{MW} \quad (1)$$

where C is the molar concentration in mol/L (Molar or M). This is also referred to as molarity, m is the mass (i.e., weight) of solute in grams (g) that must be dissolved in a volume V of the solution to make the desired molar concentration (C) and MW is the molecular weight in g/mol.

The refractive index of the salty and sugary solutions was measured with a (BOECO Digital ABBE Refractometer)

The sensor arm was immersed in these salty and sugary liquids with different concentrations and the transmission spectrum was collected and analyzed using OSA.

3. Results and discussion

It is observed experimentally through the refractometer that the refractive index increases with increasing the concentration of sodium salt or sugar in water, as shown in Figure 3.

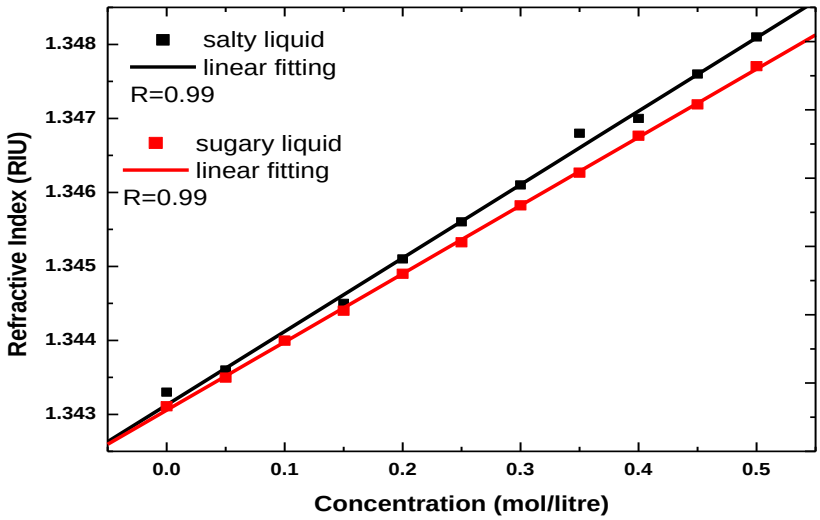

Figure 3. Refractive index variation with concentration

The different diameters of optical fibers due to different etching times were obtained and illustrated in Table 1.

Table 1. The variation of the etched fiber diameter with immersion time

Fiber no.	Etching time (minute)	Etched fiber diameter (μm)
1	60	63.5
2	90	51.58
3	120	39.68
4	150	20

The diameter of the fiber in the area exposed to HF decreases during the etching process. According to the following reaction formulas, HF reacts to silica:

$SiO2+4HF \rightarrow SiF4+2H2O$

$SiO2 +6HF \rightarrow H2SiF6 + 2H2O$

The first formula dominates the reaction concerning the present work, while the second formula dominates acid circumstances with a high concentration. Instead of tapering, this method adjusts the cladding properties while keeping the core intact [14].

Since HF has known for its ability to dissolve silica, it became evident from experience that the length of etching time required was about 150 minutes and through the etching results in Table.1 of the fibers. The remaining fiber thickness was apparent from the fibers of (39.68) μm and (20) μm fiber diameter with etching times of (120) and (150) min, respectively. Remember that the core is (9) μm in diameter. Due to figure 4, the effect of changing the refractive index of the surrounding environment of the sensor arm on the optical properties of the transmission spectra was studied for the standard fiber diameter (125 μm). The sensor arm was immersed in distilled water, and from figure 4 one can notify a noticeable wavelength shifting towards the longer wavelength due to applied distilled water to sensing arm.

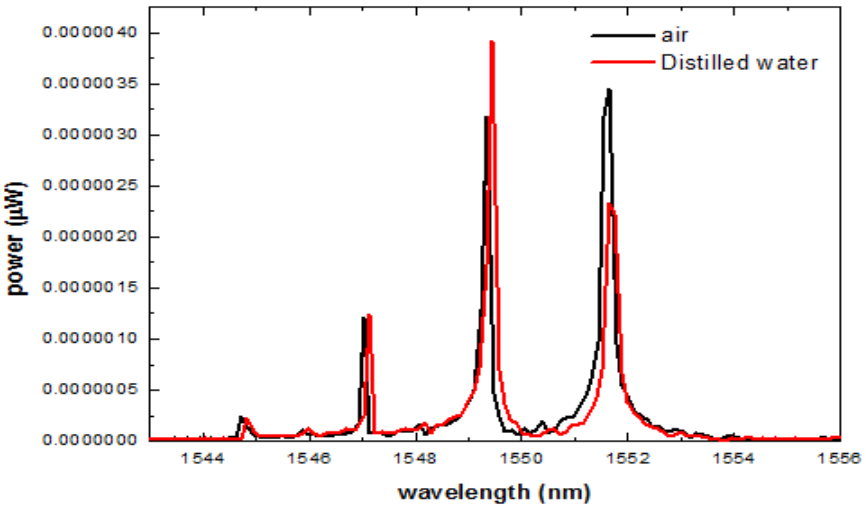

Figure 4. The transmission spectrum of air and Distilled Water

To test the system as a refractive index sensor, the sensor arm was immersed with different solutions; salt NaCl and Sugar $C_{12}H_{22}O_{11}$ with different concentrations ranging from (0 - 0.45) for both liquids. Figure 5 shows the transmission spectra of salty and sugary liquids at different concentrations.

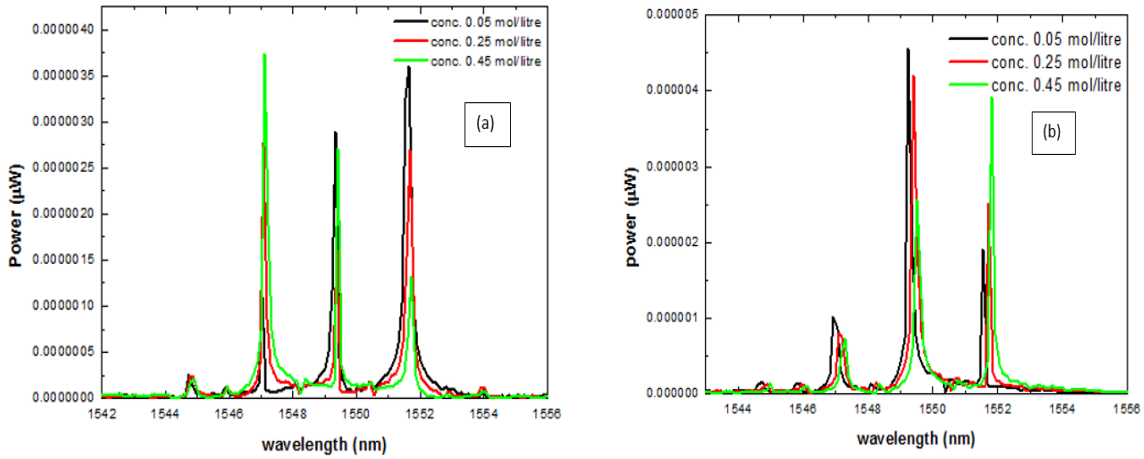

Figure 5. The transmission spectrum of (a) salty liquid, and (b) sugary liquid with selective concentrations

Figure 6 shows the linear relationship between changing in liquid concentration and shifting in the peak wavelength. The figure illustrates that the sensor shows a good sensitivity which is calculated from the linear fitting line and is equal to (202) and (220) mol/liter for salty and sugary liquids respectively.

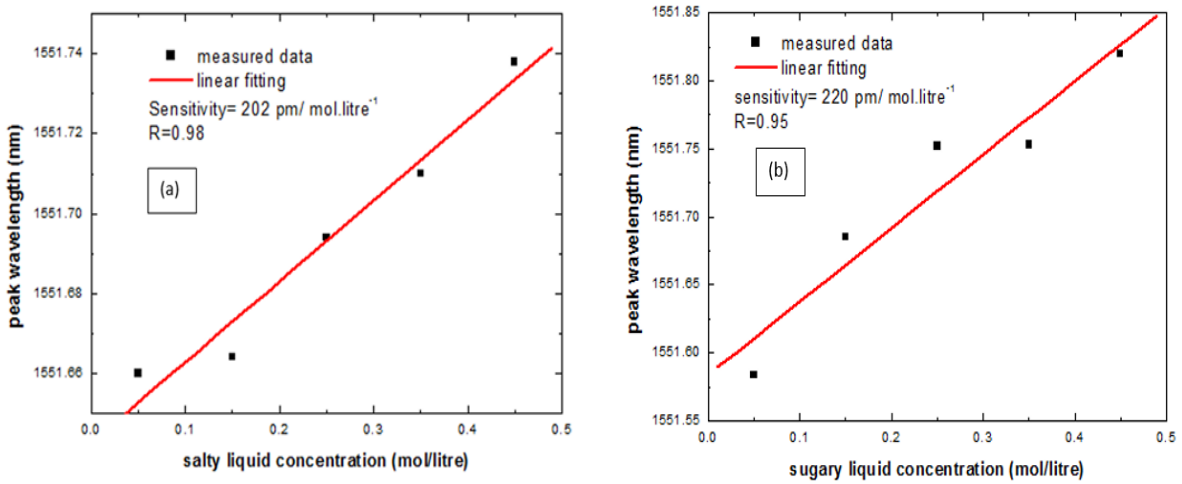

Figure 6. The relationship of peak wavelength shifting with liquid concentration for a selective peak, (a) salty liquid, (b) sugary liquid

The effect of sensor arm diameter on sensing performance had been studied. Different fiber with average diameters (63.5, 51.58, 39.68, and 20) µm were utilized and immersed in the sensing region with salty and sugary liquids with different concentrations.
Figure (7) shows the transmission spectra of salty liquid with different concentration for fiber average diameters (a) 63. 5 µm, (b) 51.58 µm, (c) 58.68 µm, and (c) 20 µm respectively.

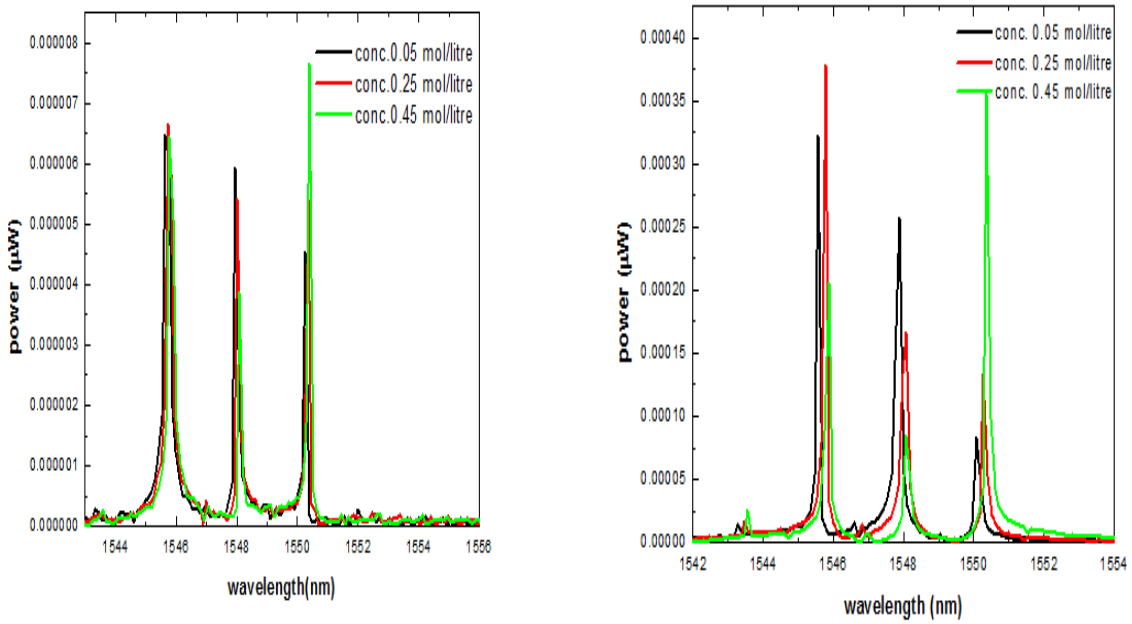

(a) *(b)*

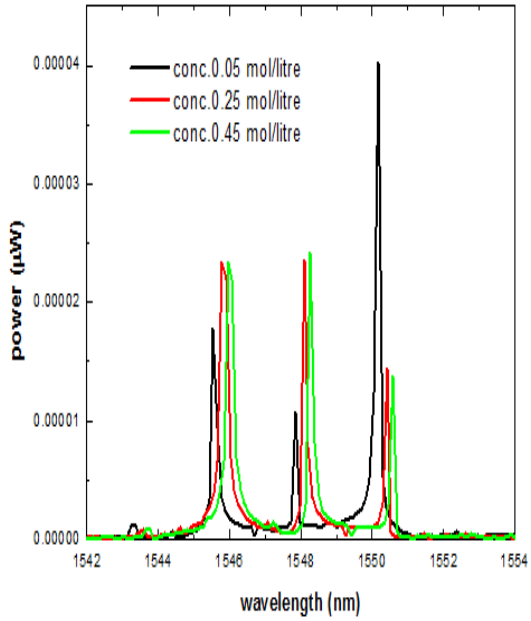

(c)

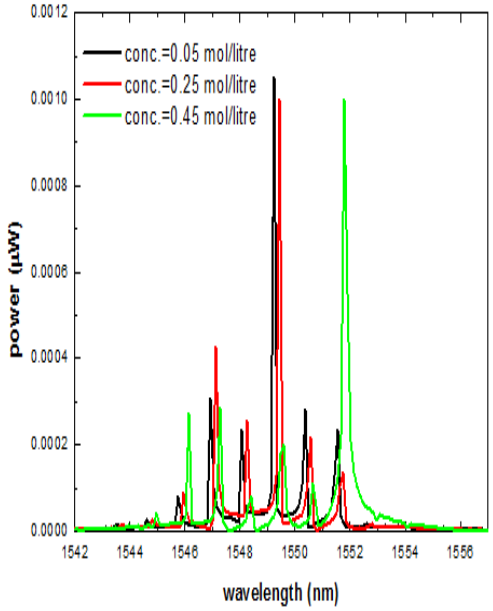

(d)

Figure 7. The transmission spectrum of salty liquid with selective concentrations with sensor diameter (a) 63.5µm, (b) 51.58µm, (c) 39.68µm, (d)20µm

Figures (8) on the other hand shows the linear relationship between the shifted in peak wavelength and liquid concentration for salty liquid with different concentration for fiber average diameters (a) 63. 5µm, (b) 51.58 µm, (c) 58.68 µm, and (c) 20 µm respectively.

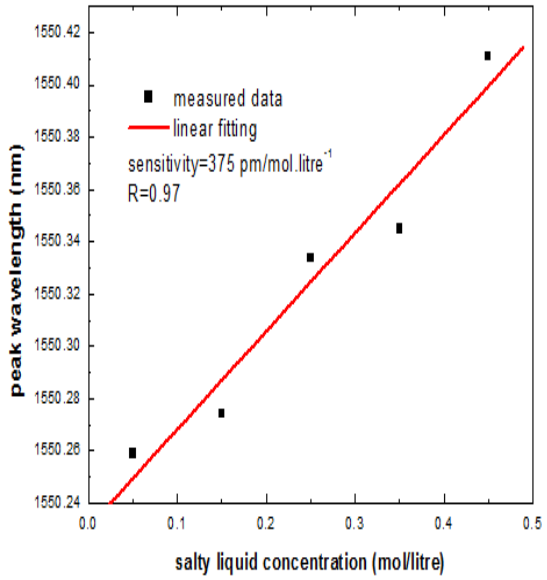

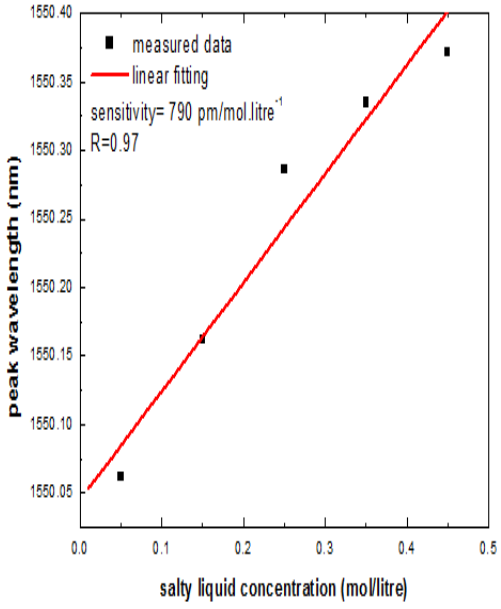

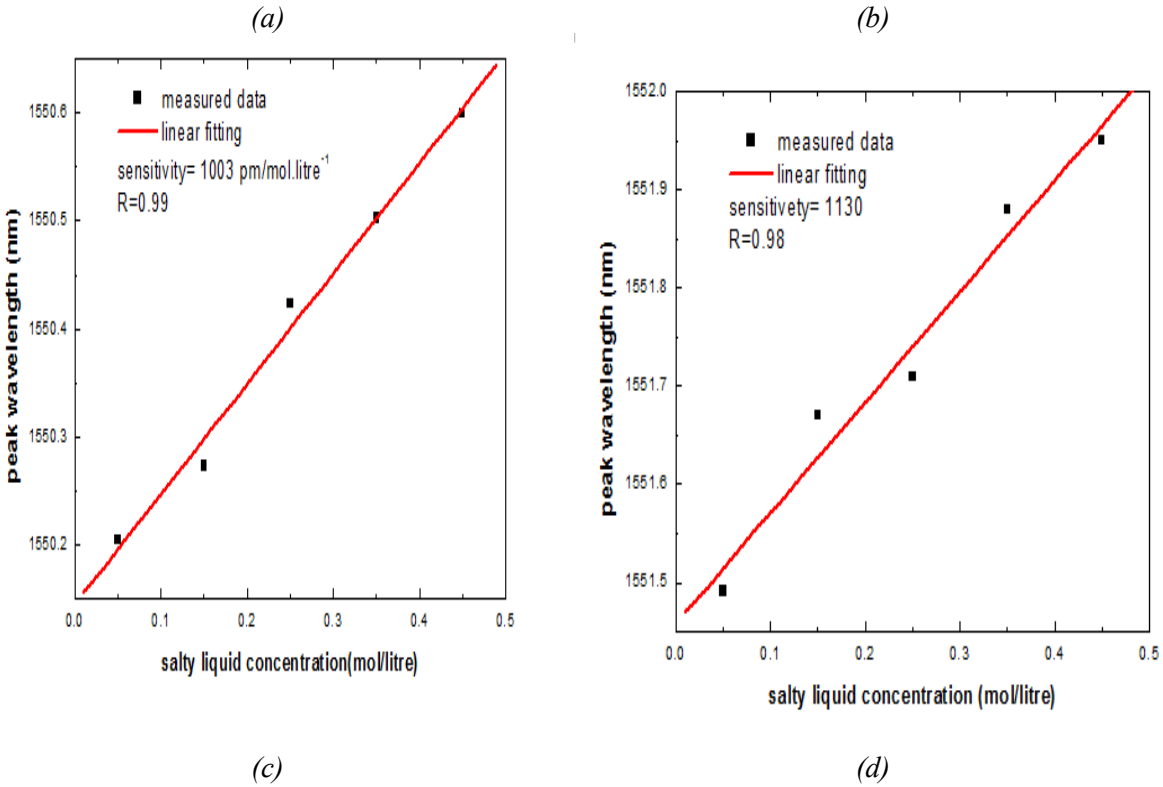

Figure 8. The relationship of peak wavelength shifting with salty liquid concentration for a selective peak, with sensor diameter (a) 63.5µm, (b) 51.58µm, (c) 39.68µm, (d)20µm

Figure (9) shows the transmission spectra of sugary liquid with different concentration for fiber average diameter (a) 63. 5 µm, (b) 51.58 µm, (c) 58.68 µm, and (c) 20 µm respectively.

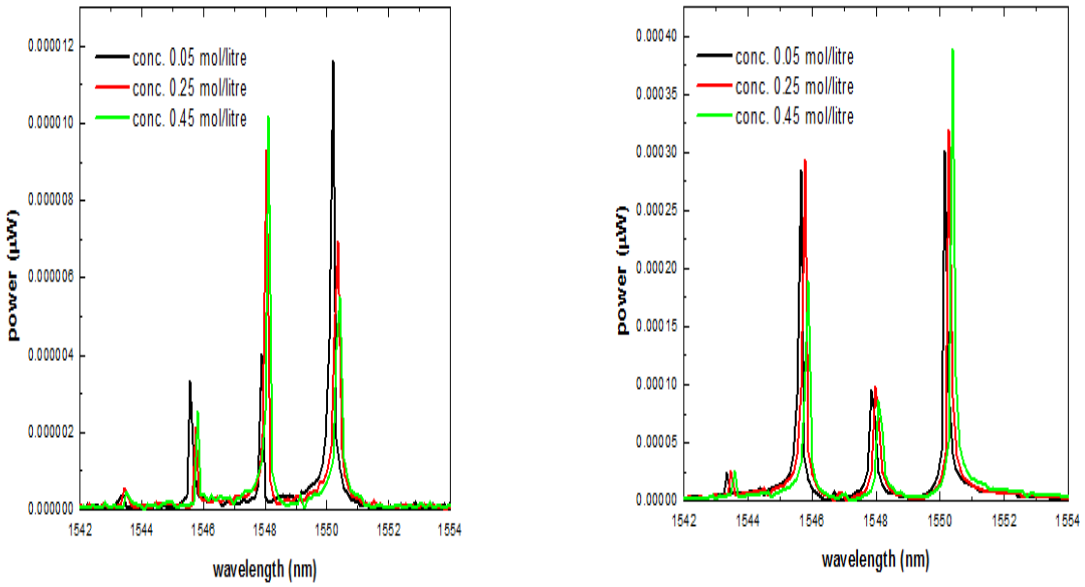

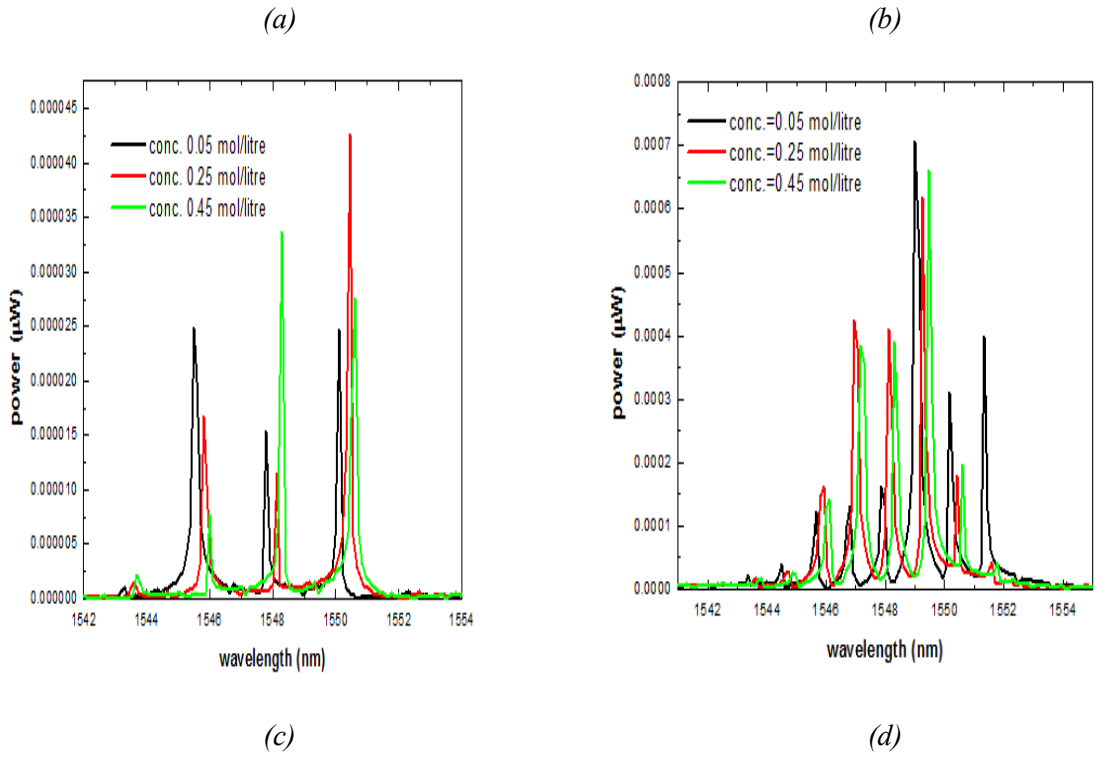

Figure 9. The transmission spectra of sugary liquid with selective concentrations with sensor diameter (a) 63.5µm, (b) 51.58µm, (c) 39.68µm, (d) 20µm

Figures (10) shows the linear relationship between the shift in peak wavelength and liquid concentration for sugary liquid with different concentration for fiber average diameter (a) 63.5 µm, (b) 51.58 µm, (c) 58.68 µm, and (c) 20 µm respectively.

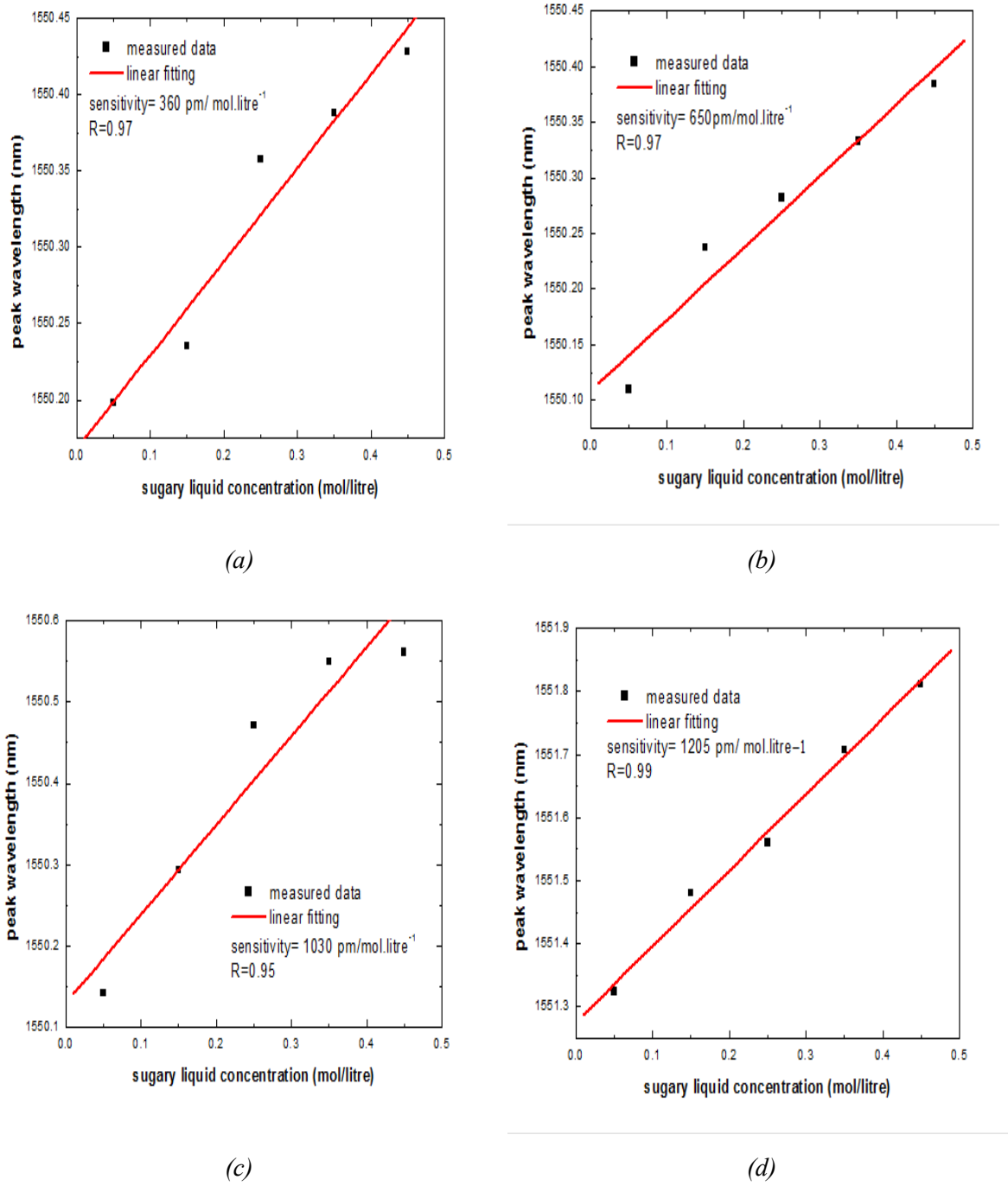

Figure 10. The relationship of peak wavelength shifting with sugary liquid concentration for a selective peak, with sensor diameter (a) 63.5µm, (b) 51.58µm, (c) 39.68µm, (d)20µm

Table (2) below shows the sensitivity of the submitted sensor for each case, from this table we can conclude that the sensor performance is enhanced as the optical fiber sensor diameter is decreased. This can be explained because the more leakage of the evanescent field from fiber cladding the more interaction with the surrounding media (liquids in this work). Also, the sensitivity values are close for

both salty and sugary liquids which declare that the type of liquid is not an important factor as its concentration on the sensing performance.

Table 2. Variation of the Sensitivity with optical fiber thickness

Fiber Dimeter (μm)	Salty liquid Sensitivity (pm/mol.litre^{-1})	Sugary liquid Sensitivity (pm/mol.litre^{-1})
125	202	220
NO.1 (63.5)	375	360
NO.2(51.58)	790	650
NO.3(39.68)	1003	1030
NO.4 (20)	1130	1205

From figures 9, 10, and Table 2 it could be noticed that the sensitivity of the submitted sensor had been enhanced by reducing the fiber diameter. The etching process leads to reduce the fiber diameter and thus strengthens the evanescent field. So, more light will be escape out of the cladding region and interact with the surrounding environments which are the salty and sugary liquids.
In standard optical fibers whose diameter is much greater than the light wavelength, the evanescent field strength at the outer surface of the cladding reduces to near zero. The light dispersed in these fibers is thus not influenced by the external environment, which decreases the interaction between the light and the sample and therefore reduces the sensitivity response of the optical fiber sensor. Carrying out the etching process and reducing the cladding thickness would allow the fibers to present large portions of ephemeral waves and surface fields of high intensity, rendering them extremely sensitive to the shift of the index to the surrounding medium by dramatically increasing the contact between directed light and the surrounding atmosphere.

4. Conclusions

The reaction activity of a Fiber Optic Evanescent Wave Sensor is greatly influenced by the thickness of the cladding within the sensing area of the fiber. We can say here that the sensor can be developed by partially removing the cladding material surrounding the optical fiber single-mode. The sensing theory, based on the variation of the refractive index based on the interaction of the transient field with the optically absorbed analyte, is utilized such that the thin cladding portion enables transmission loss by the vanishing waves that radiate energy from the heart as a function of the environment. It can also be claimed from the findings that the lower the cladding thickness, the greater the sensitivity efficiency of the optical fiber. In the field of environmental detection, such as water pollution, this sensor may be used.

Reference

[1] Kumar P Suresh et al 2002 Journal of Optics A: Pure and Applied Optics **4** (3) 247.
[2] Bansal L 2004 Development of a fiber optic chemical sensor for detection of toxic vapors.
[3] Moś Joanna E et al Crystals **9** (6) 306.
[4] Haddock Hong S Shankar P M and Mutharasan R 2003 Materials Science and Engineering: B **97**(1) 87.
[5] Zhang, Lei Jingyi Lou and Limin Tong 2011 Photonic Sensors **1** (1) 31.
[6] Polynkin Pavel et al 2005 Optics Letters **30** (11) 1273.
[7] Godin Jeremy Robert 2015 Development of an Analytical Model for a Fiber Optic Evanescent Wave Sensor.

[8] Han Xiaopeng et al 2019 Sensors **19** (24) 5440.
[9] Harris Jeremie et al 2015 Sensors and Actuators B: Chemical **206** 246.
[10] Tiwari Divya et al 2017 Sensors and Actuators B: Chemical **242** 645.
[11] Afzal Nehal S Mukherjee A and Manju Devi D 2018 International Journal of Engineering & Technology **7** (4.38) 880.
[12] Ahsani Vahid et al 2019 Sensors **19** (7) 1652.
[13] Kenza A Ferria K and Bouzid S 2020 JOSA B **37** (11) A253.
[14] Coelho L et al 2015 Plasmonics **10** (2) 319-327.

.